Sindh Univ. Res. Jour. (Sci. Ser.) Vol. 50 (3D) 24-35 (2018)

SINDH UNIVERSITY RESEARCH JOURNAL (SCIENCE SERIES)

Power Electronics Intensive Solution for Integrated Converters and Ignition System for Plug-In-Vehicles

M. BATOOL, S.A. SAJJAD[++] B. A. BAKAR*, A. ALI*

University of Engineering and Technology Taxila, Pakistan

Received 10th June 2018 and Revised 15th September 2018

Abstract: It's a big challenge for system designers to power today's portable world. Battery's use as a quality power source is on peak. Plug-in-hybrid vehicles, electric vehicles and the hybrid vehicles are being manufactured by the automotive manufacturers for improving fuel economy and reducing emissions. This paper proposes the bidirectional power converter stage for igniting the car when its battery is exhausted. This paper also proposes the efficient integration of the converter which is bidirectional in the company of a solo stage charger which is of the type i-e on-board. This concept is proved by simulating, having limitation of power i-e 20 kW while operating in propulsion mode plus 8.4kW while operating in charging mode, the design and corroborating it at a variety of power stages. The maximum efficiencies that are obtained by operation of regenerative braking is 95% and that of propulsion operation is 97%.

Keywords: Integrated chargers, electric vehicles, hybrid electric vehicle, plug in hybrid electric vehicles (PHEV's)

1. INTRODUCTION

Power electronic technology is rapidly developing over the past few years and many research efforts have centred on meliorating the economy and the functioning of electric vehicles. For further reduction of greenhouse gas emissions plug-in-hybrid electric vehicles (PHEVs), hybrid vehicles and electric vehicles are introduced (Raghavan, *et. al,* 2012), (Ghorbani, *et. al,* 2010). Electrical and mechanical components compose PHEVs. Conventional hybrid vehicles can be converted into plug in hybrid vehicles (Emadi, *et. al,* 2008), (Jones, *et. al,* 2005).This conversion can be attained by substituting the battery pack of HEV or by addition of a greater energy battery set to extend all-electric-range (Jones, *et. al,* 2005).The pack of batteries, having the capacity to store more energy can be electrically charged from external means and the other source to charge battery is regenerative braking. The stored energy is supplied in the direction of electric traction system. Charging through the means of A.C supply ineluctably needs a battery charger (Wang, *et. al,* 2005), (Egan, *et. al,* 2007), (Lee, *et. al,* 1995), (Solero, *et. al,* 2001), (Aguilar, *et. al,* 1997) along with the rectification of power factor (Mohan, *et. al,* 2003). Derived from proper current visibility for high energy battery and ac/dc converter, battery charger has various configurations. In most of PEV's this converter be positioned between propulsion machine inverter and battery (Wei, *et. al,* 2012), (Aharon, *et. al,* 2011), (Camara, *et. al,* 2012), (Garcia, *et. al,* 2006),(Park,*et. al,* 2013). The formal structure presenting the converter used for charging is ac/dc and two-way while the dc/dc converter is functional during propulsion. The system would be more effective, squeeze and cost-efficient if the bidirectional converter, used during cruising and acceleration, is integrated with add-on charger unit (Onar, *et. al,* 2012), (Ahmed, S.F, *et al*, 2014). The proposed converter is used for conversion of PEVs to PHEVs.

The system can be made more efficient if the remaining energy which is stored in car battery and store it in super capacitor's bank. With the purpose of starting the engine as soon as the voltage for battery of the car falls below the rated value require for ignition, the bank of super capacitors act as substitute power source. In this paper a bidirectional power converter stage is also developed which consists of buck and boost stages.

The proposed converter is more efficient than the other integrated chargers presented in literature (Lee, *et. al,* 2009), (Chen, *et. al,* 2011), (Dusmez, *et. al,* 2012).

The range of voltage for solo stage charging includes $120V_{AC}/220V_{AC}/240V_{AC}$ due to boost charging potential, while the battery voltage ranges are 300-400V. Incorporated converter is instanced in **(Fig 1).**

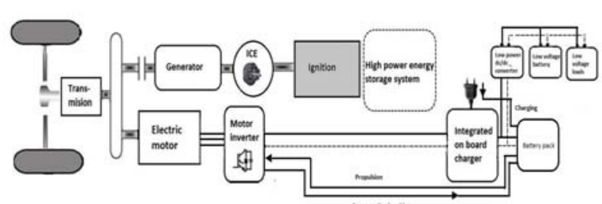

Fig. 1 System stage configuration for parallel power train of a PHEV with on-board affix battery charger and system of ignition.

The paper is ordered in this manner: In Section no. II initiation and categorization of HEVs and PHEVs and conversion of HEVs to PHEV is presented. In

[++]Corresponding author: Syeda Aneela Sajjad email: aneelashah@ciit.net.pk

*University Kuala Lumpur, Malaysia

Section no. III, the motivation is being discussed to integrate the bidirectional dc/dc converters and introducing the single stage structure in spite of two stage structured charger. There is discussion on working modes for the integrated topology in Section no. IV. In Section no. V, judgment of the converter that is proposed, on the basis of previous knowledge about the other solo-staged chargers is presented. In Section no. VI simulation and experimental results are given. In Section no. VII conclusions which are drawn are presented.

2. BACKGROUND

The hybrid vehicles have different stuff to extract energy from such as through flywheel, battery etc. as roots of energy and battery, engine, ultra capacitor, fuel cell, etc. as source of power. Reliant on vehicle form two or else further of these energy or power source can be exercised. Hybrid electric vehicles are classed as series and parallel hybrid vehicles. A series Hybrid can offer minimum fuel burning up for the duration of driving through city while a parallel hybrid can offer a minimum consumption of fuel during highway driving cycle. Hybrid vehicle can also be divided into mild, classified as of having parallel or series configuration and it power hybrids etc. (Walters, *et. al,* 2001). Plug in hybrid electric vehicle be also have battery set, the capacity to store more energy that could be charged using the charger which is on-board and through the external a.c outlet (Williamson, *et. al,* 2005), (Williamson, *et. al,* 2006), (Williamson, *et. al,* 2007), (Amrhein, *et. al,* 2005), (Katrasnik *et. al,* 2007). So as to increase effectiveness of HEVs, conversion of HEVs in PHEVs is done by many companies. So as to charge the battery from an AC outlet the battery's charger consisting of digital controller that can be programmed and an ac/dc converter with correction of power factor is desired. For transfer of energy among traction motor and battery a two-way dc/dc converter is needed.

2.1 Motivation for Integrating the Single Phase Configuration

The two-directional dc-dc converter is integrated with the charger to make system more compact. The propulsion machine is connected through inverter which is intended to work with maximum and minimum voltages. As the DC link voltage is lower, than dc/dc boost edge is obligatory and if the voltage is higher than dc/dc buck interface selected.

At low speed, the appliance is supposed to induce lesser back emf, so a boost operation is required to confine every single one of the regenerative braking power. The function of rotating magnetic field is back emf.

The volumetric and gravimetric power density is enhanced through integration of bidirectional charger by en suite dc/dc converter. Through reduced number of capacitors and inductors the cost and size of power electronic interfaces is decreased.

The chargers of battery comprised of stages of power that are two in number. To maintain the power factor as unity is to shape the grid current this is objective of first current during charging. (Chen, *et. al,* 2005), (Khaligh, *et. al,* 2012) while the second phase influences the battery stage (Gautam, *et. al,* 2012), (Liu, *et. al,* 2013). The single phase converter has uncomplicated structure, higher effectiveness and minimum parts. The unregulated current waveform is the only drawback; the little frequency portion of battery's current vibrates with double the frequency of grid. (C&D Technologies, *et. al,* 2012), (A Ali, *et. al,* 2016). Regardless of the battery's current low frequency oscillation, single phase charger topologies are favored due to reduced size and less weight.

3. MATERIAL AND METHODS

3.1 Operating Modes and Integrating Topology

The proposed integrated topology comprises of four switches by way of body diodes, one diode bridge, four diodes and one inductor. Battery operates between the input power sources of 120/220/240V_{ac}, 300.0V and 400.0V is the range for variation of voltage.

The controller for charger is able to incorporated to the controller for motor with the feedback that is achieved through the voltage feeler positioned on grid's face of unreceptive rectifier.

The proposed topology has different modes of process that is regenerative braking, ignition, charging and propulsion. The stepping-down and stepping-up operations both are possible during regenerative braking propulsion. The power converter stage consists of buck and boost operations for igniting the car.

The switches' states in each method are summed up in **(Table 1),** whereas opposite indication for PWM is presented as PWM'.

Table 1: Modes of operation and succession of switches

Operation mode	Energy flow	Mode	No	S1	S2	S3	S4	D5	D6	D7	D8
Propulsion	$V_{bat}-V$	BOOST	1	PWM	OFF	ON	OFF	-	-	-	PWM'
propulsion	$V_{bat}-V$	BUCK	2	OFF	OFF	PWM	OFF	-	PWM	-	ON
Regenerative breaking	[illegible]	BOOST	3	OFF	PWM	OFF	ON	-	-	PWM'	-
Regenerative breaking	[illegible]	BUCK	4	OFF	OFF	OFF	PWM	PWM'	-	ON	-
Charging	[illegible]	BOOST	5	OFF	PWM	OFF	OFF	-	-	PWM'	-
Ignition	$V_{bat}-V$	BUCK	6	-	-	-	ON	PWM'	-	-	-
Ignition	$V_{bat}-V$	BOOST	7	ON	-	-	-	-	-	-	PWM

3.1.1 Mode 1: Operation of Boost starting at the affix battery to the HV-Bus of PEV throughout propulsion

The operation of Boost starting at the HV-Bus of PEV to the affix battery throughout propulsion is shown in **(Fig. 2).**

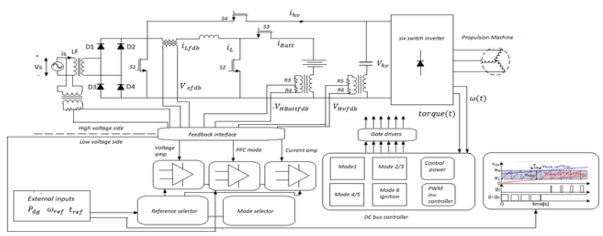

Fig. 2. Incorporated Topology

For such an operation, *S*1 is the main boost switch and *S*3 is turned ON. Beginning through the affix battery towards the HV bus the power know how to be approximated via calculated battery voltage and current and so the movable power at a definite status of charge be supposed to governed properly. When the switch *S*1 is ON, the energy is stored in inductor and at the same time energy is supplied to motor through an inverter via capacitor. The inductor provides energy to motor by forcing *D*8 to carry out current and charge the HV bus *C*hv

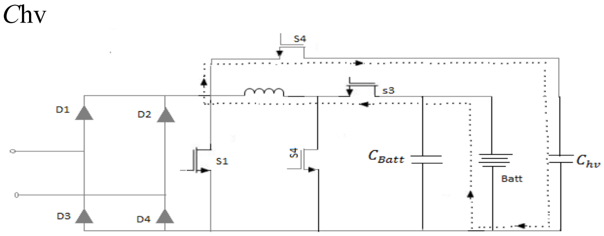

Fig. 3(a)

3.1.2 Mode 2: Operation of Buck over Propulsion mode of PEVs

*S*3 works for PWM switching, while all other switches remains in the OFF state, and a free-wheeling passageway is provided by *D*6. Switches *S*1, *S*2, *S*4 and diodes *D*4 and *D*5 follow the OFF condition. The stimulant voltage reference provides vigor to the load and inductor when *S*3 became ON. When *S*3 is turned OFF, energy channelized towards the load and D6 is forward biased. The flow of energy is on or after battery to the inverter in all modes during propulsion i-e buck, boost modes.

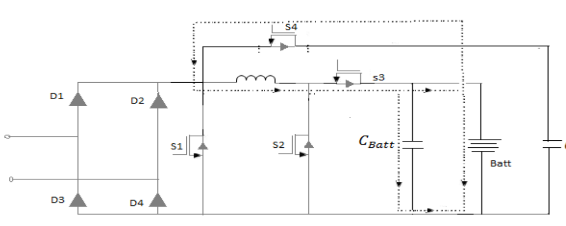

Fig. 3(b)

3.1.3 Mode 3: Operation of Boost over Reg. Braking of PEV

There is an additional advantage of boosting ability during operation of regenerative braking i-e getting the power at low speeds. The energy will be lost if the boosting interface is not present; when in urban traffic vehicle is driven at low speeds because at that time the yielded voltage crossways the propulsion mechanism is minor. The distance between conduction times is given away in **(Fig 3 c).**The boost and buck working manners of reg. braking analogous to those of propulsion manner but in the opposite direction.

In this mode *S*2 works for switching the PWM, *S*4 remains in the ON condition and the other switches represents the OFF condition.

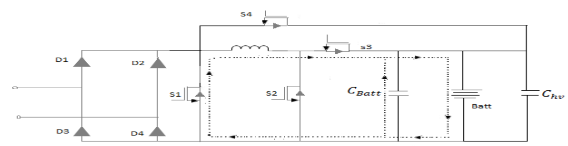

Fig. 3(c)

3.1.4 Mode 4: Operation of Boost over Reg. Charging of the Affix Battery of PEVs.

At high speeds, the highest braking energy produced; induces highest voltage around the ends of propulsion mechanism; vital mode during that time is the buck operation. The circuit operation in this approach is made known in Fig 3(d).At inverter output, the eminent voltage is stepped down by switching *S*4.

Through *D*7 the energy is transmitted from dc bus that is of eminent voltage to the battery and the inductor keeps energy by a voltage of Vi-V0. The capacitor discharged over the battery and the inductor's energy transmitted to the battery.

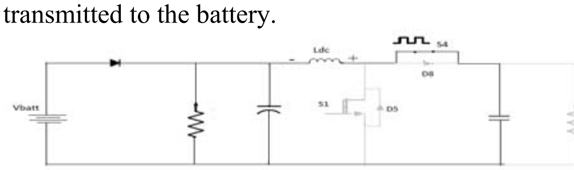

Fig. 3(d)

3.1.5 Mode 5: For Plug-In Charging of the Affix Battery Non inverting Boost–Buck process

The inductor stores energy when switch *S*2 is ON, established by the practical contributed voltage. In the meantime, energy is provided to load via capacitor linked towards battery and *D*1 and *D*4 are carrying on the current. Depending on the input grid voltage, diodes *D*2 and *D*3 will conduct. The operation of incorporated charger is like an ac-dc PFC boosting rectifier. The procedure for charging is revealed in **(Fig. 4)**. Under the *V*grid – *V*bat influence, the inductor current decreases and *D*7 is impelled to conduct when *S*2 is turned to be OFF. Meanwhile, capacitor parallel to battery is charged.

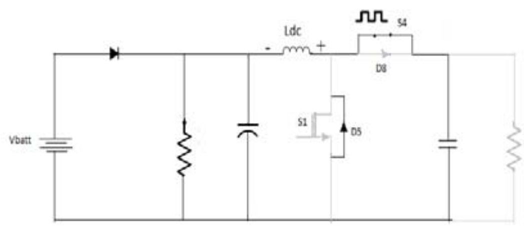

Fig 3(e)

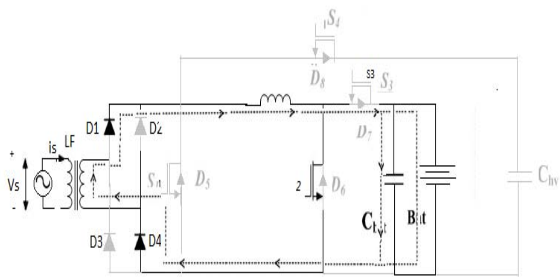

Fig. 4. Charging mode

3.1.6 Mode 6: Buck Mode during Ignition

During state 1 (T_{ON}), switch $S4$ is turned ON and linked to inductor, and the biasing of diode $D5$ is reverse. For that reason, the energy is supplied to the inductor L_{DC} and load through the input capacitor. In mean time, energy is supplied by battery via $D8$ to the inductor. During state 2 (T_{OFF}), $S4$ switch is OFF biasing of diode $D5$ is of forward type. The path of current of an inductor stay unaffected As a result, the current of an inductor surge all the way to diode $D5$ and from the inductor energy is still transmitted to load

As switch $S4$ is ON, there is increase inI_L. The inductor voltage VL is greater, given that the energy is being store in inductor openly. At what time $S4$ switch is turned OFF, there is decrease in I_L .The energy which is given to the load is supplied by the inductor. For that reason, the output voltage $V0$ is kept invariant.

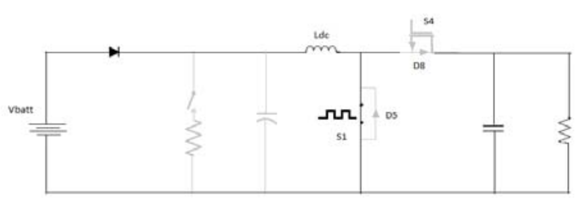

Fig 3(f)

3.1.7 Mode 7: Boost Mode during Ignition

During state 1 (T_{ON}), $S1$ switch represents ON state and linked to the ground, diode $D8$ is reverse biased. In the meantime, through $D7$, battery supplies the energy to inductorL_{DC}. In state 2 (T_{OFF}), the switch $S1$ is OFF diode $D8$ represents the forward biasing state, as a result amount of voltage produced is connected to L_{DC} once more and established energy as of L_{DC} in addition to the contribution from input. Around $S1$, voltage Vs is less when $S1$ is in the ON state, by reason of the current across inductor I_L is greater than before. On basis of the source current I_s that supplies the energy to inductor I_L enhances. There is no course approaching output, of current, via diode whose current is nil. As soon as $S1$ is switched OFF, the Vs across $S1$ is greater, I_L is reduced in view of the fact that the accumulated energy will discharge towards the load. As the switch $S4$ is OFF then I_s is nil. Therefore, the output voltage $V0$ is kept invariant.

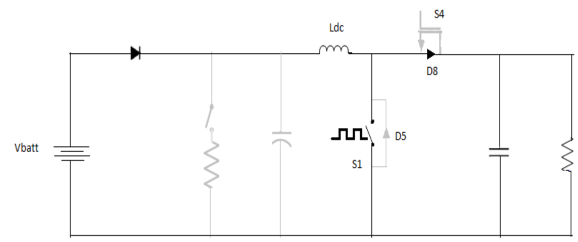

Fig 3(g)

3.2 Relative Study of the Bidirectional Converter

3.2.1 Proportional Assessment with Other Solo-Staged Charger Structures

The proposed integrated topology is compared with other solo-staged charger specifically inverting buck-boost rectifier, Boost PFC rectifier, positive buck/boost rectifier and semi active boost rectifier. These are potential non isolated single-stage structures. The comparison of these topologies is given in Table II. The dc-dc converter connecting the battery and the dc bus having higher voltage is compared with four-quadrant two-directional buck-boost topology which is shown in Fig. 5. From table II, the converter which is suggested is put side by side with the other solo staged chargers and concluded that the number of semiconductors devices are minimum and requires only one current feeler for all modes of action together with PFC.

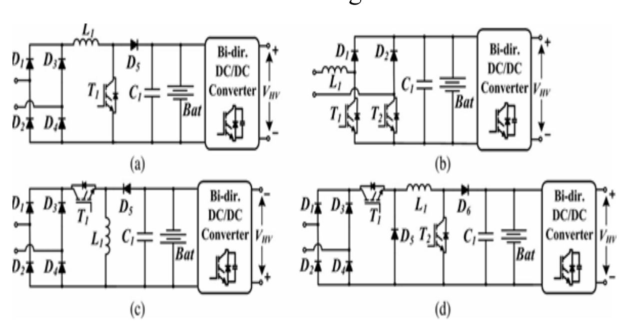

Fig. 5. Potential solo-staged add-on charger topologies: (a) PFC boost rectifier, (b) semi active dual PFC boost rectifier, (c) inverting buck/boost PFC rectifier

Table 2: comparison of other solo-staged chargers with incorporated charger

Charger topologies	Battery voltage range	Voltage polarity	Switch /Body's Diode	Diode	Current sensor	Inductor
Boost PFC rectifier	$V_{grid,peak}$-	+	4+1	5	2	1+1
Semi active dual boost	$V_{grid,peak}$-	+	4+2	2	2	1+1
Inverting Buck/ Boost	$V_{grid,peak}$-	-	4+1	5	2	1+1
Positive Buck/ Boost	$V_{grid,peak}$-	+	4+2	6	2	1+1
Integrated charger-1[14]	$V_{grid,peak}$-	+	6	9	1	1
Integrated charger2 [15]	$V_{grid,peak}$-	+	9	0	1	1
Proposed charger	$V_{grid,peak}$-	+	4	4	1	1

3.2.2 Diminution of Size of PEV by reason of exclusion of Inductor

For the quantification of the diminution of size by eradication of involved charger, the reference values for charging in uninterrupted mode of conduction CCM is precisely enlighten in **(Table 3).**

Table 3: terms of the involved charger

Specifications	Values
Output power(P_{out})	8400W
Switching frequency(f_{sw})	20,000Hz
Battery voltage range (V_{Batt})	300V-400V
Minimum input voltage (V_{in})	200V-260V
Maximum peak to peak current ($\Delta I_{peak,peak}$)	6500mA
Maximum efficiency of the charger(η_{ch})	92%

In order to validate the size of core of the charger that is of on-board type, first we need is to find out the value of critical inductance for uninterrupted mode of conduction.

The equation for critical inductance is:

$$L_{cr} = \sqrt{2}V_{in,min}\left(1-\frac{\sqrt{2}V_{in,min}}{V_{bat\_max}}\right)/f_{sw}\Delta I_{pk\_pk} \quad (1)$$

The second parameter, which is important for determination of core size, is the energy calibration, through the given equation:

$$E = \frac{L_{cr} I_{in\_pk}^2}{2} \quad (2)$$

In the equation above, the value of I_{in-pk} is calculated by the equation given below:

$$I_{in\_pk} = \frac{\sqrt{2}P_{out}}{V_{in,min}\eta_{ch}} + \frac{\Delta I_{pk\_pk}}{2} \quad (3)$$

Now, we are at the stage where we know the energy saving requisite plus value of critical inductance intended for an inductor, here volume of core able to be estimated by analysis of magnetic course. Ampere's rule establishes relation involving flux density *B*, turns ratio *n,* length of magnetic track *lm*, and of the magnetic path permeability μ as:

$$I_{max} = \frac{B_{max} l_m}{n\mu} \quad (4)$$

As shown from equation above there is direct relation between flux density *B*max and maximum current *I*max when current reaches its maximum value *I*max then maximum density of flux *B*max is accomplished. The core material *B*max maximum flux density must be greater than the saturation flux density *B*max got through current. The greatest current that can be passed through the core without causing any damage to core is given by equation below:

$$I_{max} = \frac{K W_a J}{N} \quad (5)$$

Here, K is window fill factor, *Wa* (cm2) is the winding area and *J* (A/cm2) is current density of the core

Permeability can be derived from (4) and (5):

$$\mu = \frac{B l}{K W_a J} \quad (6)$$

Faraday's Law, used to express the magnetic circuit's energy storage potential, named as inductance as:

$$L = \frac{N^2 A_c \mu}{l} \quad (7)$$

Substituting (6) and (7) in (2) to get $W_a A_c$:

$$W_a A_c = \frac{2E}{B_{max} K J} \quad (8)$$

The above equation shows that there is inverse relation between core volume and saturation flux density. The core material determines the flux density. The maximum flux density is 15600 G, for an unstructured core made of iron (Powerlite, *et. al,* 2011). If the tolerable flux density is 14000 G while fill factor is 14000 G and the current density is 500 A/cm2 then the core area product is 105 cm4.

For estimating the volume for the required *Wa*Ac Power Lite cores are analyzed (Powerlite, *et. al,* 2011). In accordance to requirements, AMCC-125 is the least sized core with the external dimension of 12.1 cm × 6.3 cm ×3.5 cm, adding up the volume of 2.66*10^5 mm3 and a weight of 1100 g devoid of windings. Thus, the converter provides 2.66*10^5 mm3 lessening of size and 1100 g weight lessening by elimination of the inductor that is PFC on the involved charger. Further reduction of magnitude is possible because of the elimination of diode and insulated-gate bipolar transistor (IGBT) rated at 80 A/1200 V as compared to fundamental charger publicized in Fig. 5(a). SOT-227 is the IGBT designed for this rating of power and diode is typically TO-247 packages in this integrated topology the weight is further reduced by the conventional control strategy elimination now the conventional controllers are not required and heat sink necessities significantly compact the weight.

3.2.3 Estimating the Change in Conduction Losses

In the proposed converter no extra loss of switching is there; seeing that simply one control switch switched at the time of conduction of one mode in the entire procedure.

The transmission loss for diode can be given as equation below:

$P_D = V_F I_F$ [In watts](Diode conduction loss) (9)

The summation of reverse recovery loss, the power dissipation and wastefulness of heat inside the resistance are termed as power loss of a diode. The knee voltage and the mean current are multiplied to get the formula of dissipation of power.

`

$$P_D = R_D I_{D,rms}^2 + V_F \cdot I_{D,ave} + P_{Q,RR} \quad (10)$$

Here, *PQ,* RR stand for the losses linked with diode's reverse recovery. Basically, it's the integration of recovery current under time. The equation for reverse recovery losses is written below:

$$P_{Q,RR} = Q_{RR} \cdot V_{out} \cdot f_{sw} \quad (11)$$

The losses of reverse recovery able to be ignored but we take buck mode into account although these losses can't be ignored when boost mode is operating.

The rms and average rating of current of diode for boost operation are given below:

$$I_{D,boost,rms} = \sqrt{I_{in}^2 \cdot (1-d) + \frac{d^2 V_{in}^2 (1-d)}{12 f_{sw}^2 L^2}} \quad (12)$$

$$I_{D,boost,ave} = (1-d) \cdot I_{in} \quad (13)$$

The dc link processed as yield in propulsion approach whereas output current and voltage quantities are related to battery voltage in regenerative braking mode, since the converter is both increasing and decreasing the voltage in direction of power surge. The diode power release in stepping down operation is calculated when the rms and the average rating of stepping down current are known, these values are calculated by formula below:

$$I_{D,buck,rms} = \sqrt{I_0^2 \cdot (1-d) + \frac{V_0^2 (1-d)^3}{12 f_{sw}^2 L^2}} \quad (14)$$

$$I_{D,buck,ave} = (1-d) I_{out} \quad (15)$$

This equation expresses the conduction loss for IGBT:

$$P_{IGBT} = V_{CE(SAT)} \times I_{s,ave} + R_C \times I_{S,rms}^2 \quad (16)$$

$$I_{S,boost,rms} = \sqrt{I_{in}^2 \cdot d + \frac{d^2 V_{in}^2}{12 f_{sw}^2 L^2}} \quad (17)$$

$$I_{s,boost,ave} = d \cdot I_{in} \quad (18)$$

While, the conduction losses of MOSFET are given as:

$$P_Q = R_{DS} \quad (19)$$

The input power is given as:

$P_{in} = P_{0/\eta_{eff}}$ [in watts]

On behalf of Mode no. 5 (plug-in charging of the affix battery), we can say that the converter have less switches and also revealed from Fig. 3(c), when put side by side with Fig.5 (a). In addition, the decrease in loss is

$\Delta P_l = P_{S3}$ [in watts]

On behalf of Mode no. 1 (Operation of Boost starting at the affix battery to the HV-Bus of PEV throughout propulsion), as exposed in Fig. 4, further one switch and diode pair is removed in the converter that is proposed, comparing with Fig. no5(c). The discrepancy in loss is

$$\Delta P_l = P_{D4} + P_{S5} \quad (20)$$

Intended for Mode 4 (Operation of Boost over Reg. Charging of the Affix Battery of PEVs) further one switch and diode pair is replaced, as given away in Fig. 3, put side by side with **(Fig. 5(b).** The difference in loss is

$$\Delta P_l = P_{D6} + P_{S3} \tag{21}$$

For the estimation of change in efficiency, *Po* is the power of output, *P*in is the old power of input, εold is the old effectiveness, and ε new is the new effectiveness. The efficiency change is given as

$$\Delta\varepsilon = \varepsilon_{new} - \varepsilon_{old}$$

The relative change in efficiency in different modes is termed as function of εold, Δ*Pl*, and *Po*:

$$\Delta\varepsilon = \varepsilon_{new} - \varepsilon_{old} = \frac{P_o}{P_{in} + \Delta P_l} - \frac{P_o}{P_{in}}$$

$$= \frac{1}{\frac{P_{in}}{P_o} + \frac{\Delta P_l}{P_o}} - \frac{P_o}{P_{in}} = \frac{1}{\frac{1}{\varepsilon_{old}} + \frac{\Delta P_l}{P_o}} - \varepsilon_{old}\%$$

In accordance to, each operating mode loss calculation is given as follows:

On behalf of Mode no. 5, given away in Fig. no. 3(a), assume operation of buck–boost for the riskiest calculation of loss

$$P_{0_{max}} = 1440W = V_{0_{min}} I_{0\_max}$$

$$I_{0\_max} = \frac{1440}{134} = 10.75A$$

FOR MOSFETS:

$\Delta P_l = P_{Q3} = I_{0\_max}^2 . R_{DS}$=5.20W

$$\Delta\varepsilon_{max} = \frac{1}{\frac{1}{\varepsilon_{old}} + \frac{5.20}{1440}} - \varepsilon_{old}$$
$$= 0.254 \sim 0.322\%$$

FOR IGBTS:

$$\Delta P_l = P_{Q3} = I_{0_{max}} . V_{CE(SAT)} = 26.86W$$

For Mode 4 In fig 3(c)

$$\Delta\varepsilon_{max} = \frac{1}{\frac{1}{\varepsilon_{old}} + \frac{26.86}{1440}} - \varepsilon_{old}$$

$= -1.176 \sim$1.486%

$$P_{0_{max}} = 5000W = V_{hv\_min} . I_{hv_{max}} = V_{batt\_min} . I_{batt\_max}$$

$$I_{hv\_max} = \frac{5000}{216} = 23.15\,A$$

$$I_{batt\_max} = \frac{5000}{134} = 37.31A$$

FOR MOSFETS:

$$\Delta P_l = P_{D4} + P_{S4}$$

$$V_F . I_{batt\_max} + I_{hv\_max}^2 . R_{DS} = 59.52W$$

$$\Delta\varepsilon_{max} = \frac{1}{\frac{1}{\varepsilon_{old}} + \frac{92.52}{5000}} - \varepsilon_{old}$$
$$= -0.754 \sim 0.954\%$$

FOR IGBTS:

$$\Delta P_l = P_{D4} + P_{S4}$$

$$V_F . I_{batt\_max} + V_{CE(SAT)} . I_{hv_{max}} = 98.28\ W$$

$$\Delta\varepsilon_{max} = \frac{1}{\frac{1}{\varepsilon_{old}} + \frac{98.28}{5000}} - \varepsilon_{old} = -1.176 \sim -1.486\%$$

In Mode 3, in Fig. 3(c)

$$P_{0\ max} = 5000 = V_{batt\ min} . I_{batt\ max}$$

$$I_{batt\_max} = \frac{5000}{134} = 37.31A \quad V_{batt\_min} = d . V_{hv\_min}$$

$$d = \frac{V_{batt\_min}}{V_{hv\_min}} = \frac{134}{216} = 0.620 \quad d' = 1 - d = 0.38$$

$$I_{hv\ max} = I_{batt\ max} . d' = 14.179A$$

FOR MOSFETS:

$$\Delta P_l = P_{D6} + P_{S3}$$

$$V_F . I_{hv\_max} + I_{batt\_max}^2 . R_{DS} = 76.11W$$

$$\Delta\varepsilon_{max} = \frac{1}{\frac{1}{\varepsilon_{old}} + \frac{76.11}{5000}} - \varepsilon_{old} = -0.962 \sim -1.216\%$$

FOR IGBT:

$$\Delta P_l = P_{D6} + P_{Q5}$$

$$= V_F . I_{hv\_max} + V_{CE(SAT)} . I_{batt\_max}$$

=106.75W

$$\Delta\varepsilon_{max} = \frac{1}{\frac{1}{\varepsilon_{old}} + \frac{106.75}{5000}} - \varepsilon_{old} = -1.348 \sim -1.697\%$$

It is shown from table that by the use of MOSFETs the Δεmax are less than 1.3% while that for IGBTs are less than 1.7%.

4. RESULTS AND DISCUSSION

The efficiency, functionality and operation of the converter that is proposed is verified through simulations performed. In **(Table 4),** the considerations for testing be established. It ought to be mentioned here that if 240 VAC is the voltage of grid then power of charging must be restricted to 8400 W.

Whenever, 400 V is the voltage selected for operation of battery, the conveyable power of dc/dc part be capable to reach 20,000 W.

Table 4: conditions for simulation

Specifications	Test condition	Limits
Maximum power during charging	1.8kW	8.4kW
Maximum power during propulsion mode	1.6kW	20kW
Maximum power during regenerative Braking mode	1.5kW	20kW
Input grid voltage	120-150VAC	0-240V
Battery voltage	130-250V	300-400V
DC link voltage	165-250V	300-450V
Inductor current	0-12.5A	50A
Switching frequency	20kHz	20kHz

20,000 Hz is fixed as frequency for switching of all processing ways. For optimized losses, this is suitable frequency and in data sheet of utilized MOSFETs use of this frequency is encouraged.

The heat is surely dissipated by MOSFETs if during charging at less power, the greater frequency of switching be able to in use.

It is known that, if the frequency for switching is greater than there are less current ripples and distortion in total harmonics is better

When switching is hard, then there is increase in losses percentile and with the increase in switching frequency efficiency decreases.

Henceforth, during charging process frequency for switching choice is a trade off among the current ripples and decreased effectiveness. Depending on, the peak current having greater value in stage of dc/dc, the thickness of inductor winding and the size of core is selected. In propulsion and charging both modes, the ripple in current which is permitted is selected on the basis of value of inductance. According to the requirement of an application this can be varied.

The size of components chooses under the design directions of dc/dc changeover phase where switching frequency is 20,000 Hz.

For the converter that is of greater power, the fall and rise time for the selected switches and diodes must be large this will be the source of intense losses of recovery seeing that more time required by the diode to recuperate. Looking on the mode of operation, the current of input/output is deformed and the losses are induced due to oscillating current in electrical device, especially in the testing of high voltages. *D*5 release over *C*hv during boost mode in propulsion at the time of *S*1 switching, roots to unwanted oscillation and considerable losses. The solution is to add the LCL filter between battery and the sides of greater voltage.

At different levels of power; boost for the duration of propulsion, charging and buck for the period of regenerative braking simulations are done. The voltage and current waveform's screenshot for the period of charging having power of 1800 W shown in **(Fig. 6).** The voltage sensor yielding 0.006 V calculates the output and input voltages.150.0 VAC is the voltage of input while 250.0 VDC is the fixed voltage of output. The current sensor measures the current of grid input. The current of DC-link recorded 6500mA while that of value of rms current is 11800 mA. The calculated efficiency is 92%.

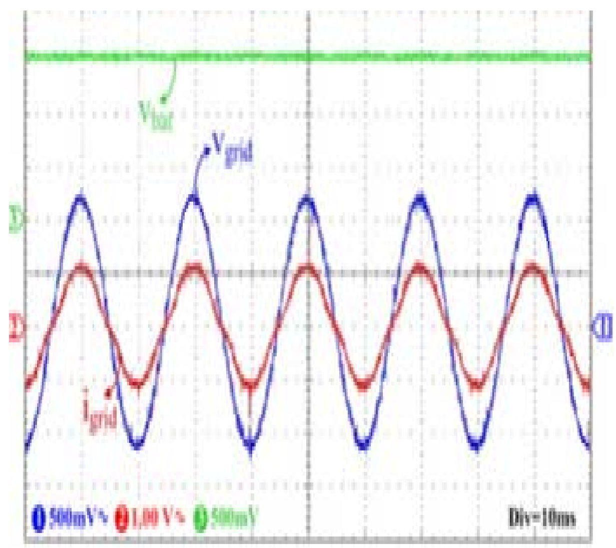

Fig. 6. Simulation waveforms for charging process (Channel 1: yield of sensor 0.006 Volt/Volt, voltage of grid [83 Volt/division]), Channel 2: yield of sensor 65 millivolt/Ampere current of grid 15 Ampere/division, Channel 3: yield of sensor 6 millivolt/Volt),

The charging mode efficiency plot demonstrated by Fig. no.7.At 1200 W the effectiveness becomes greater to 92% curvature .At different levels of power i-e 240W to 1600W the propulsion boost is simulated. 165 VDC is the voltage of battery part. Although there is enhancement in load for every analysis the objective of control is to maintain 250 VDC the voltage of output.

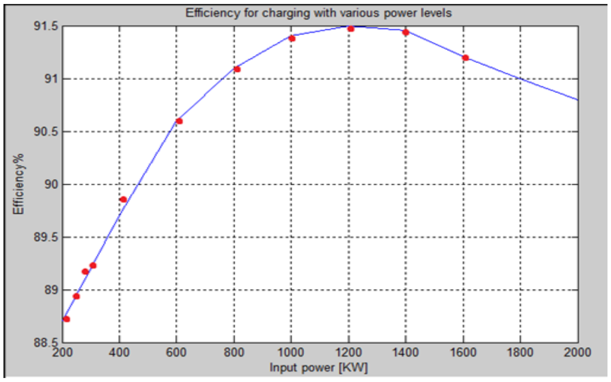

Fig. 7. Curve for efficiency during charging operation

The upholding of voltage of output is the main objective of control stage although there is enhancement in load for every analysis 250 VDC The oscilloscope screenshot in propulsion boost demonstrated in **(Fig. 8)**. The 0.1V/A current is deliberated by probes. At 250 V. subsequent to 1600 W power dc current of bus is confirmed as 6400 mA. At 165 V the current of battery side is recorded as 10170 mA. The efficiency of this test is recorded as 96%.

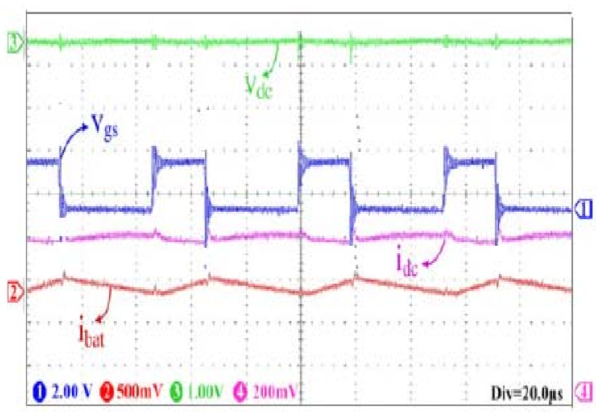

Fig. 8. Simulation waveforms of boost approach during propulsion (Channel 1: signal of gate [20 Volt/division], Channel 2: battery side current [5 Ampere/division] probe outputs100 milliVolt/A, Channel 3: dc bus voltage [165 Volt/division] sensor outputs 6 millivolt/volt, Channel 4:dc bus current [2 Ampere/division] probe output (100millivolt/Ampere).

The current of inductor rises by a unvarying slope on turning ON switch. Due to the filters at output there is smooth and continuous the current of the dc bus. In the voltage of dc-connection little spikes are observed. By reason of, the losses in reverse recovery in switching case and in charge the efficiency decreases.

This know how to be surmount in the course of active techniques of soft-switching for instance switching of zero-current-zero-voltage and with switches that are faster in the direction of lessening the losses of switching, predominantly the losses of reverse recovery.

The effectiveness curve the converter against power output with 250 V voltage of bus that is dc and 165 V battery's voltage considered and obtainable in **(Fig. 9).**

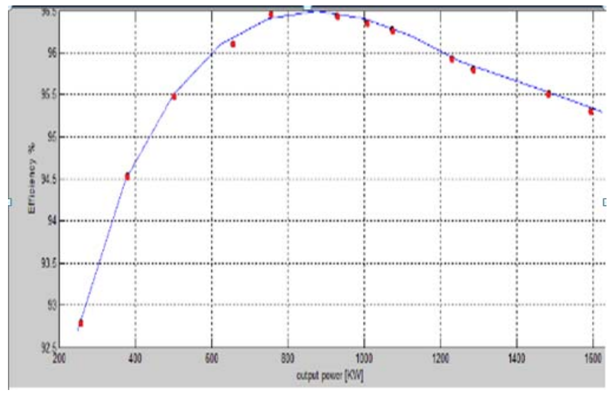

Fig. 9. Curve of Efficiency in boost during propulsion

At 250 W the effectiveness is 92%, at 750 W boosts to 96% power of output, and afterward at 1600 lessens to 95%. The reg. braking of buck operation screenshot is given in **(Fig. 10).** 170 V is the bus voltage of dc and intended to buck it to 120 V. As 12500mA is the current of battery side then 9600mA is the bus current of dc. Towards the battery side, 1500W is the power conveyed, while 1632 W is the power considered as of the dc bus. The effectiveness is calculated as 92%.

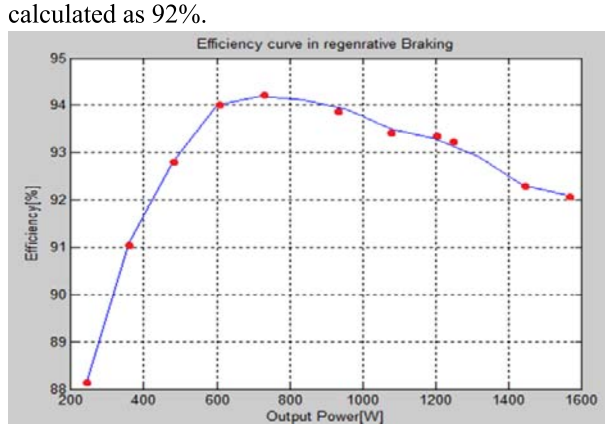

Fig. 10. Curve for efficiency of reg. braking

Through 11 points of testing having 170 V as voltage of dc bus and 120 V as the voltage of battery face, is the extraction of effectiveness curve and draw through polynomial of sixth-order shown in fig. no. 11. At loads that are not heavy, the effectiveness is the least and boost up to 95%. Since 12500mA is the amplified battery face current, the effectiveness drop off a bit to 91.90%.

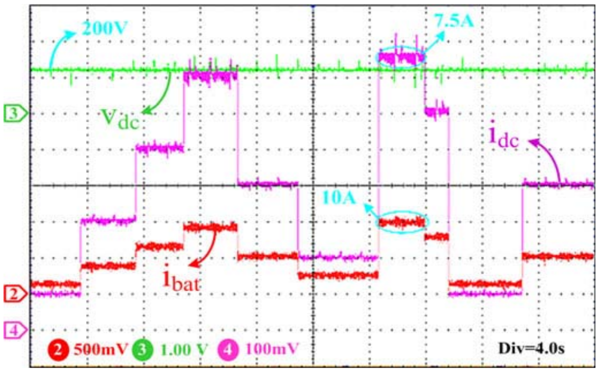

Fig. 11. Vibrant response of the converter to variations of load in boost propulsion way (Channel 2: probe outputs 100 milliVolt/Ampere, battery side current [5 Ampere/division] Channel 3: sensor outputs 6 milliVolt/Volt, bus voltage of dc [165 Volt/division] Channel4:probe output 100 millivolt/Ampere, bus current i-e dc (1 Ampere/division)

The consequences are given in **(Fig. 12)** for blocked control - loop of reg. braking approach of buck within the link of dc voltage changes. The dc voltage is assorted physically linking 0.130mV and 0.165m V. The current of battery face is keeping up at 0.004 m A while the voltage of battery side is unvarying at 0.120m V. The controller effectively maintains the current of battery side yet the voltage of input changes piercingly. The ripple in the current of inductor becomes greater, even if the typical current of inductor stay the same as the voltage of input become greater. Owing to the actuality that inductor voltage *V*in – *Vo* becomes greater as the increase in *V*in as the switch is ON. In view of the fact that the load at the output is fixed, through scheming the current of battery side, voltage of battery face is in line too. The current or voltage parameter is similar to the power parameter at the fixed power applications of load. There is decrease in the current input accordingly to keep up 480 W when the voltage of input becomes greater

.

Resembling blocked-loop management of the stepping-up operation in propulsion, a blocked-loop voltage management is to be done for maintaining the voltage 120 V of battery side. These results are presented in Fig no. 18. A small number of voltage spikes are pragmatic voltage in the battery face due to switching.

The influential reaction of the system that is blocked-loop screenshot are prearranged. At 250 V there is effective adjustment by controller still through transitions of quick load. There is change in current 1000mA to 7500mA of dc-link yet, at the instance of quick load deviations the effectiveness is 92%, at 750 W boosts to 96% power of output, and afterward at 1600 lessens to 95%. Through 400 W to 1500 W, the control maintains the voltage still at 250 V.

In **(Fig.12)** the buck mode state results during ignition system is shown and in figure no. 13 the results of boost mode during ignition is shown.

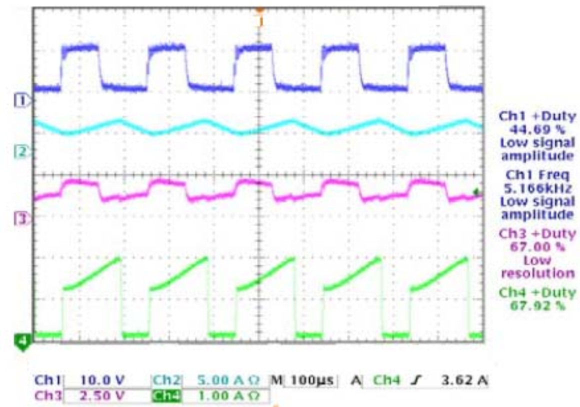

Fig. 12. Buck Mode during Ignition

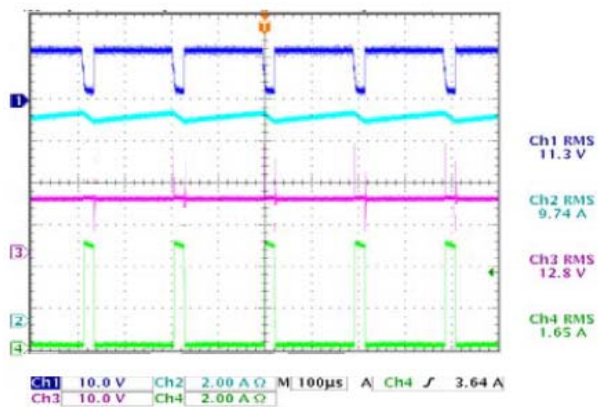

Fig. 13. Boost Mode During Ignition

5. CONCLUSION

An incorporated single-stage charger and two-way dc-dc converter for PEV apps have been demonstrated here. The anticipated system also has another power converter stage for igniting the car. This topology hence obviates the requirement of other power adaptation stages for charger so there is reduction in size and weight of the interfaces. There is 266 cm3 and 1.10 kg lessening for charger having an 8.40 kW power by the removal of the inductor's core accompanying two different power electronics converters in favor of power factor correction. The proposed topology is compared with the other existing topologies and its advantages are mentioned. Changes in conduction losses are described and effectiveness due to extra switches and diodes one-time addressed. Simulations done to verify the operating modes i-e buck mode during propulsion, boost mode during propulsion, plug-in attached battery charging, buck and boost operation approach during ignition. The controller chooses the strategy to control and for the proper operation of modes in accordance to the input-output voltage and current variations. The peak efficiency for the charging is 92%, for propulsion is 97%, and for regenerative braking is 95%.On the basis of the accomplished results, the purported converter is an effective and compact system with no issues of ignition system for available and next-generation PEVs.

REFERENCES:

Aguilar, C., F. Canales, J. Arau, J. Sebastian and J. Uceda (1997) “An integrated battery charger/ discharger with power-factor correction,” IEEE Trans. Ind. Electron, vol. 44, no. 5, 597–603.

Amrhein. M., and P. T. Krein, (2005). “Dynamic simulation for analysis of hybrid electric vehicle system and subsystem interactions, including power electronics,” IEEE Trans. Veh. Technol., vol. 56, no. 3, 825–836.

Aharon. I., and A. Kuperman, (2011). “Topological overview of power trains for battery-powered vehicles with range extenders,” IEEE Trans. Power Electron., vol. 26, no. 3, 868–876.

Ahmed. S. F., (2014): "Model Predictive Controller-based, Single Phase Pulse Width Modulation (PWM) Inverter for UPS Systems." ACTA Polytechnica Hungarica 11.6 23-38.

Ali. A.,. S. F. Ahmed, M. K. Joyo, A Malik, M Ali, K Kadir, Z. M. Yusof, (2016) Sindh University Research Journal-SURJ (Science Series) 48 (4D), 79-82

Chen. H., X. Wang, and A. Khaligh, (2011). “A single stage integrated bidirectional AC/DC and DC/DC converter for plug-in hybrid electric vehicles,” in Proc. IEEE Veh. Power and Propulsion Conf., 1–6.

Camara. M. B., B. Dakyo, and H. Gualous, (2012). “Polynomial control method of DC/DC converters for DC-bus voltage and currents management- Battery and supercapacitors,” IEEE Trans. Power Electron., vol. 27, no. 3, 1455–1467.

Dusmez. S., and A. Khaligh (2012) “A novel low cost integrated on-board charger topology for electric vehicles and plug-in hybrid electric vehicles,” in Proc. App. Power Electron. Conf., Feb., 2411–2616..

Egan. M. G., D. L. O’Sullivan, J. G. Hayes, M. J. Willers, and C. P. Henze, (2007). “Power-factor-corrected single-stage inductive charger for electric vehicle batteries,” IEEE Trans. Ind. Electron., vol. 54, no. 2, 1217–1226.

Emadi. .A., Y. J. Lee, and K. Rajashekara, (2008). “Power electronics and motor drives in electric, hybrid electric, and plug-in hybrid electric vehicles,” IEEE Trans. Ind. Electron., vol. 55, no. 6, 2237–2245.

Ghorbani, R., E. Bibeau, and S. Filizadeh, (2010) “On conversion of hybrid electric vehicles to plug-in,” IEEE Trans. Veh. Technol., vol. 59, no. 4, 2016–2020.

Garcia. O., P. Zumel, A. de Castro, and A. Cobos, (2006). “Automotive DC/DC bidirectional converter made with many interleaved buck stages,” IEEE Trans. Power Electron., vol. 21, no. 3, 578–586.

Gautam. D., F. Musavi, M. Edington, W. Eberle, and W. G. Dunford, (2012). “An automotive on-board 3.3 kWbattery charger for PHEV application,” IEEE Trans. Veh. Technol., vol. 61, no. 8, 3466–3474.

Jones, W. D., (2005). “Take this car and plug it [plug-in hybrid vehicles],” IEEE Spectr., vol. 42, no. 7, 10–13.

Katrasnik. T., F. Trenc, and S. R. Opresnik, (2007). “Analysis of energy conversion efficiency in parallel and series hybrid powe rtrains,” IEEE Trans. Veh. Technol., vol. 56, no. 6, 3649–3659.

Khaligh. A., and S. Dusmez, (2012). “Comprehensive topological analysis of conductive and inductive charging solutions for plug-in electric vehicles,” IEEE Trans. Veh. Technol., vol. 61, no. 8, 3475–3489.

Lee, Y J., A. Khaligh, and A. Emadi, (2009). “Advanced integrated bidirectional AC/DC and DC/DC converter for plug-in hybrid electric vehicles,” IEEE Trans. Veh. Technol, vol. 58, no. 8, 3970–3980.

Liu. C., B. Gu, J. Lai, M. Wang, Y. Ji, G. Cai, Z. Zhao, C. Chen, C. Zheng, and P. Sun, (2013). “High-efficiency hybrid full-bridge-half-bridge converter with shared ZVS lagging leg and dual outputs in series,” IEEE Trans. Power Electron., vol. 28, no. 2, 849–861.

Mohan. N., T. M. Undeland, and W. P. Robbins, (2003). Power Electronics: Converters, Applications, and Design, 3rd. Hoboken, N J: Wiley.

Honnyong, P. Z. Fang, and L. M. Tolbert, (2012). “55-kW variable 3X DC-DC converter for plug-in hybrid electric vehicles,” IEEE Trans Power Electron., vol. 27, no. 4, . 1668–1678.

Onar. O. C., J. Kobayashi, D. C. Erb, and A. Khaligh, (2012). “A bidirectional high-power-quality grid interface with a novel bidirectional noninverted buck-boost converter for PHEVs,” IEEE Trans. Veh. Technol., vol. 61, no. 5, 2018–2032.

Park. T., and T. Kim, (2013). “Novel energy conversion system based multimode single-leg power converter,” IEEE Trans. Power Electron., vol. 28, no. 1, 213–220.

Powerlite Inductor Cores, Datasheet. (2011). [Online]. Available: http:// www.hitachimetals.com/ product / amorphous / powerlite in ductorcores documents /POWERLITE_C_opt.pdf

Raghavan. S. S., and A. Khaligh, (2012). "Electrification potential factor: Energy based value proposition analysis of plug-in hybrid electric vehicles," IEEE Trans. Veh. Technol., vol. 61, no. 3, 1052–1059,

Sul. S. K., and S. J. Lee, (1995). "An integral battery charger for four-wheel drive electric vehicle," IEEE Trans. Ind. Appl., vol. 31, no. 5, 1096–1099.

Solero, J.,. L. (2001). "Nonconventional on-board charger for electric vehicle propulsion batteries," IEEE Trans. Veh. Technol., vol. 50, no. 1, 144–149.

Technologies, (2012). Charger output AC ripple voltage and the effect on VRLA batteries, Tech. Bulletin. [Online]. Available: http://www.cdtechno.com/pdf/ref/41_2131_0212.pdf

Wang.C. S., O. H. Stielau, and G. A. Covic, (2005) "Design considerations for a contactless electric vehicle battery charger," IEEE Trans. Ind. Electron., vol. 52, no. 5, 1308–1314.

Walters. J., H. Husted, and K. Rajashekara, (2001). "Comparative study of hybrid powertrain strategies," in Proc. SAE Future Transp. Technol. Conf., Costa Mesa,
Williamson S. S. and A. Emadi, (2005). "Comparative assessment of hybrid electric and fuel cell vehicles based on comprehensive well-to-wheels efficiency analysis," IEEE Trans. Veh. Technol., vol. 54, no. 3, 856–862.

Williamson. S. S., S. M. Lukic, and A. Emadi, (2006). "Comprehensive drive train efficiency analysis of hybrid electric and fuel cell vehicles based on motor controller efficiency modeling," IEEE Trans. Power Electron., vol. 21, no. 3, 730–740.

Willamson, S. S., A. Emadi, and K. Rajashekara, (2007)."Comprehensive efficiency modeling of electric traction motor drives for hybrid electric vehicle propulsion applications," IEEE Trans. Veh. Technol., vol. 56, no. 4, 1561–1572.

Wu. T., J. Hung, S. Tseng, and Y. Chen, Feb. (2005). "A single-stage fast regulator with PFC based on an asymmetrical half-bridge topology," IEEE Trans. Ind. Electron., vol. 52, no. 1, 139–150.